PCCP

PAPER

View Article Online
View Journal | View Issue

Cite this: *Phys. Chem. Chem. Phys.*, 2025, **27**, 16254

Impacts of molecular architecture on the radiation-induced degradation and reaction kinetics of hydrophobic diglycolamides with the solvated electron and the dodecane radical cation†

Michaela R. Bronstetter, *[abc] Gregory P. Horne, *[c] Andrew R. Cook, [d] Stephen P. Mezyk, [e] Joseph R. Wilbanks, [c] Bobby Layne, [d] Alyssa Gaiser [ab] and Jacy K. Conrad *[c]

Given their proposed use as trivalent actinide–lanthanide separation ligands, the role of molecular architecture on the radiation robustness of diglycolamide (DGA) molecules has been investigated. This study examined three prototypical molecules with differences in their aliphatic chain architecture: *N*,*N*,*N*′,*N*′-tetra(*n*-octyl)diglycolamide (TODGA), *N*,*N*,*N*′,*N*′-tetra(2-ethylhexyl)diglycolamide (T2EHDGA), and *N*,*N*′-dimethyl-*N*,*N*′-dioctyldiglycolamide (DMDODGA). Rate coefficients and activation parameters are reported for the reactivity of each DGA with the solvated electron (e_{solv}^-) and the corresponding dodecane radical cation ($RH^{\bullet+}$) over the temperature range of 10.0 to 44.1 °C. These measurements indicate that DMDODGA is the most chemically reactive with both transient radicals, which may be attributed to this molecule's more accessible backbone. Complementary gamma dose accumulation studies (≤ 600 kGy) under envisioned process conditions—50 mM DGA in *n*-dodecane solvent—afforded dose constants for the loss of DGA of d = (3.41 ± 0.07) × 10^{-3}, (4.19 ± 0.09) × 10^{-3}, and (4.65 ± 0.09) × 10^{-3} kGy^{-1} for T2EHDGA, DMDODGA, and TODGA, respectively. These dose constants indicate that varying DGA architecture affords subtle differences in chemical reactivity, leading to varying rates of radiolytic degradation under envisioned actinide–lanthanide separation conditions. However, more ambitious DGA frameworks, such as modifying the backbone, branching of the aliphatic chains, and/or changing the size of the chain may be required for larger gains in radiolytic longevity while optimizing actinide–lanthanide selectivity.

Received 7th April 2025,
Accepted 3rd June 2025

DOI: 10.1039/d5cp01332a

rsc.li/pccp

Introduction

The recovery of uranium and plutonium from used nuclear fuel (UNF) is essential for achieving a sustainable fuel cycle that maximizes energy production and resource utilization from each fuel assembly, whilst minimizing the long-term radiotoxic burden on waste storage facilities and repositories. Traditionally, these elements have been recovered using solvent extraction processes that employ selective ligands dissolved in an organic diluent (*e.g.*, *n*-dodecane or odorless kerosene) to complex and extract the uranium and plutonium from an acidic aqueous phase containing UNF.[1] However, these processes typically do not extract the trivalent minor actinides (MAs), americium and curium, leaving them in the aqueous phase. These rejected MAs contribute to the long-term radiotoxicity and thermal burden of nuclear waste. The recovery of the MAs is complicated by the presence of fission product lanthanides (Ln), which are also predominantly trivalent ions with similar ionic radii. Efficiently separating these elements while enhancing established industrial extraction processes has been extensively investigated.[2–10] Many

[a] *The Facility for Rare Isotope Beams, Michigan State University, East Lansing, MI 48824, USA. E-mail: bronstet@msu.edu*
[b] *Department of Chemistry, Michigan State University, East Lansing, MI 48824, USA*
[c] *Center for Radiation Chemistry Research, Idaho National Laboratory, 1955 N. Fremont Ave., P.O. Box 1625, Idaho Falls, ID 83415, USA. E-mail: jacy.conrad@inl.gov*
[d] *Department of Chemistry, Brookhaven National Laboratory, Upton, New York 11973, USA*
[e] *Department of Chemistry and Biochemistry, California State University Long Beach, 1250 Bellflower Boulevard, Long Beach, California 90840-9507, USA*

† Electronic supplementary information (ESI) available: Arrhenius plot for the reaction of DGAs with the dodecane radical cation ($RH^{\bullet+}$). Steady-state gamma irradiation of DGA derivatives. 1 mM DGA derivative kinetics with the solvated electron (e_{solv}^-). 2 mM DGA derivative kinetics with the solvated electron (e_{solv}^-). 3 mM DGA derivative kinetics with the solvated electron (e_{solv}^-). 4 mM DGA derivative kinetics with the solvated electron (e_{solv}^-). 1 mM DGA derivative kinetics with the dodecane radical cation ($RH^{\bullet+}$). 2 mM DGA derivative kinetics with the dodecane radical cation ($RH^{\bullet+}$). 3 mM DGA derivative kinetics with the dodecane radical cation ($RH^{\bullet+}$). 4 mM DGA derivative kinetics with the dodecane radical cation ($RH^{\bullet+}$). DGA concentration determination after gamma radiolysis *via* gas chromatography-flame ionization detection (GC-FID). See DOI: **https://doi.org/10.1039/d5cp01332a**

advanced flowsheets from this research propose the use of diglycolamide (DGA, Fig. 1A) extractants for MA removal, which have demonstrated high MA and Ln distribution ratios under highly acidic conditions.

An essential factor in developing efficient and economic UNF reprocessing technologies is the radiolytic robustness of a ligand. The radiation-induced destruction of a ligand and concomitant formation of its degradation products typically limit the effectiveness and longevity of a reprocessing solvent system.[11–17] For instance, the primary degradation pathways identified for DGA radiolysis are illustrated in Fig. 1A with cleavage at the O_{ether}–C_{ether} bond being the most common mode.[12,18–21]

These pathways lead to the formation of *N*,*N*,*N*′-trioctyldiglycolamide (TrODGA), 2-hydroxy-*N*,*N*′-dioctylacetamide (DOHyA), and *N*,*N*-dioctylacetamide (DOAA) from the radiolysis of *N*,*N*,*N*′,*N*′-tetra(*n*-octyl)diglycolamide (TODGA, Fig. 1B). The accumulation of these degradation products has been attributed to a progressive decrease in MA and Ln distribution ratios with increasing absorbed gamma dose.[22] The radiolytic degradation of various extractants has been studied to identify chemical parameters, such as solvent system composition, metal ion complexation, and molecular architecture, which can be controlled to enhance their radiolytic longevity and separations performance under scalable process conditions.[10–12,18,21–42]

Irradiation of ligands in organic media affords the formation of multiple excited species and reactive radicals from solvent radiolysis:[13,32,43]

$$RH \rightsquigarrow e_{solv}^{-}, RH^{\bullet+}, RH^{*}, R^{\bullet}, H^{\bullet}. \quad (1)$$

Previous studies have indicated that the early stages of ligand degradation are triggered by primary species formed by ionization of the solvent, namely the solvated electron (e_{solv}^{-}) and solvent radical cation ($RH^{\bullet+}$).[12,19,21] As a result, the predominant basis of ligand degradation can be correlated to the extent to which a DGA molecule reacts with the e_{solv}^{-} and $RH^{\bullet+}$ to form radical ions ($DGA^{\bullet-}$ and $DGA^{\bullet+}$) in competition with their charge recombination process to form a solvent excited state (RH^{*}):[12,19]

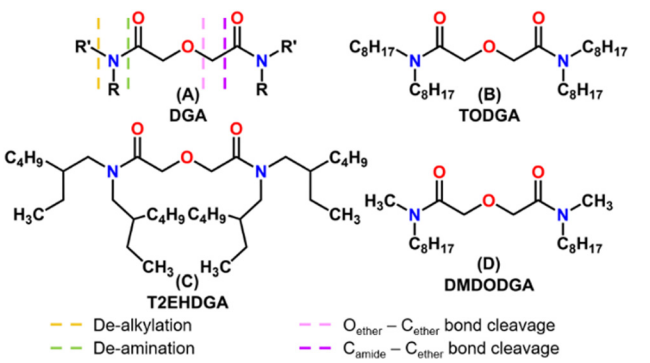

Fig. 1 Diglycolamide backbone structure (DGA, A), with commonly reported diglycolamide degradation pathways and their respective corresponding colored dashed lines (- -). Derivatives studied here: *N*,*N*,*N*′,*N*′-tetra(*n*-octyl)diglycolamide (TODGA, B), *N*,*N*,*N*′,*N*′-tetra(2-ethylhexyl)-diglycolamide (T2EHDGA, C), and *N*,*N*′-dimethyl-*N*,*N*′-dioctyldiglycolamide (DMDODGA, D).

$$DGA + e_{solv}^{-} \rightarrow DGA^{\bullet-}, \quad (2)$$

$$DGA + RH^{\bullet+} \rightarrow DGA^{\bullet+} + RH, \quad (3)$$

$$e_{solv}^{-} + RH^{\bullet+} \rightarrow RH^{*}. \quad (4)$$

Therefore, understanding these mechanisms and their kinetics is critical for the tailored design of DGA molecules with a lower chemical affinity for these radical species or subsequent chemistry that limit the extent of radiation-induced ligand damage and the formation of problematic degradation products. Several reports address the interactions between the $RH^{\bullet+}$ and TODGA,[12,19,31,32,44] but equivalent reactions for other DGAs or with the e_{solv}^{-} remain unexplored, even though the e_{solv}^{-} has the same radiolytic yield as the $RH^{\bullet+}$.

Many lipophilic DGAs have demonstrated relatively long lifetimes in radiation environments.[12,45–47] For instance, TODGA has a reported radiation dose constant of $d = (4.10 \pm 0.30) \times 10^{-3}$ kGy^{-1} in neat *n*-dodecane solvent.[12] Modifications in a DGA's molecular architecture have been found to influence its radiolytic longevity;[39,45–47] specifically, incorporating branching chains into a DGA alkyl chain increases its radiation-resistance.[45–47] For example, Deepika *et al.*[45] reported a dose constant of $d = 0.43 \times 10^{-3}$ kGy^{-1} for *N*,*N*,*N*′,*N*′-tetra(2-ethylhexyl) diglycolamide (T2EHDGA, Fig. 1C) in *n*-dodecane, indicating an order of magnitude greater radiation resistance compared to TODGA. Additionally, Galán *et al.*[39] observed that substituting labile C–H bonds with stronger C–C bonds on a DGA backbone may enhance durability and radiation robustness; however, there were discrepancies with one or two substitutions of a methyl group to the backbone. Conversely, Zarzana *et al.*[12] reported similar dose constants for the gamma irradiation of TODGA and T2EHDGA in *n*-dodecane, concluding that further study on varying the length of a DGA aliphatic chain is unnecessary.[12]

In this study, we examined the time-resolved and dose accumulation effects of molecular architecture on the fundamental radiation chemistry of the DGA framework, specifically comparing TODGA, T2EHDGA, and *N*,*N*′-dimethyl-*N*,*N*′-dioctyldiglycolamide (DMDODGA, Fig. 1D). T2EHDGA features a hexyl aliphatic chain with a branching ethyl group, resulting in the same number of carbons but more steric bulk compared to TODGA. DMDODGA, on the other hand, has R-groups consisting of one methyl group and an octyl chain on either side of the DGA, offering less steric hinderance than both TODGA and T2EHDGA. Considering that the overall rate of ligand degradation in organic media is initiated by reactions involving the e_{solv}^{-} and $RH^{\bullet+}$, we report new second-order rate coefficients (k, M^{-1} s^{-1}) and kinetic activation parameters (Arrhenius, E_a and A) for TODGA, T2EHDGA, and DMDODGA as a function of temperature (10.0–44.1 °C). This is the first study to report such data for the e_{solv}^{-} reaction with any separations ligand in organic media. Additionally, we present new gamma radiolysis dose constants for each DGA in *n*-dodecane under cobalt-60 gamma irradiation to resolve discrepancies between previously reported studies.

Methods

Materials

N,*N*,*N*′,*N*′-Tetra(*n*-octyl)diglycolamide (TODGA, 97.0%), *N*,*N*,*N*′,*N*′-tetra(2-ethylhexyl)diglycolamide (T2EHDGA, ≥97.0%), and *N*,*N*′-dimethyl-*N*,*N*′-dioctyldiglycolamide (DMDODGA, ≥97.0%) were supplied by Marshallton Research Laboratories, Inc. (Piedmont Triad, North Carolina, USA). Iron(III) sulfate heptahydrate ($FeSO_4{\cdot}7H_2O$, ≥99.0%), *n*-dodecane (≥99.0% anhydrous), *n*-hexane (≥97.0% HPLC), sodium chloride (NaCl, 99.999% trace metals basis), sulfuric acid (H_2SO_4, 99.999%), and triethylamine (TEA, ≥99.5%, GC) were obtained from MilliporeSigma (Burlington, Massachusetts, USA). Argon (Ar) and nitrous oxide (N_2O) compressed gases were purchased from Airgas (Radnor, PA, USA) with purities ≥99.5%. All chemicals were used without further purification.

Time-resolved electron pulse irradiations

Chemical kinetics were determined for the reactions of TODGA, T2EHDGA, and DMDODGA with the e_{solv}^- and $RH^{\bullet+}$ in *n*-dodecane using the Brookhaven National Laboratory (BNL) Laser Electron Accelerator Facility (LEAF). The LEAF transient absorption detection system has been described previously.[48] This study utilized ∼10 ps electron pulses with both FND-100Q (EG&G, silicon, 200–1000 nm) and GAP-300 (GPD Optoelectronics Corp, Salem, New Hampshire, InGaAs, 900–1600 nm) photodetectors with and without a signal amplifier (FAST ComTec, Germany, TA1000B-10, 1 GHz), in conjunction with a Teledyne LeCroy (Chestnut Ridge, NY, USA.) Waverunner 6Zi 600 MHz transient digitizer, affording a final system time resolution of 1 ns.

Samples comprised of varying concentrations of each DGA (≤4 mM) dissolved in argon-sparged neat *n*-dodecane. The e_{solv}^- decay was measured at 1600 nm, where it absorbs strongly.[49] The decay kinetics of the $RH^{\bullet+}$ were followed at 850 nm, the maximum of its absorption spectrum.[50] Both sets of reaction kinetics were measured at 10.0, 20.0, 30.0, and 44.1 ± 2.0 °C to obtain the corresponding kinetic activation parameters. Temperature control was achieved by placing sample cuvettes in a custom brass sample holder installed at the end of the LEAF beamline. The sample holder was insulated by a 3D printed adapter and monitored using a K-type thermocouple (Omega Engineering, Norwalk, CT, USA) placed next to the sample cuvette. A mixture of propylene glycol and water from a refrigerator circulating bath (Lab Companion RW-0525G, Billerica, Massachusetts, USA) was used to regulate the sample holder temperature. The cuvette's temperature was calibrated with a separate K-type thermocouple directly inserted into a cuvette filled with ethanol to ensure actual sample temperatures before and after each DGA set and to offset the bath temperature as needed.

Dosimetry was determined at the beginning of each day by measuring the absorption of the hydrated electron (e_{aq}^-) in an aqueous solution (with 1 M NaOH and 20% methanol) at 650 nm (G_ε = 7.2 × 10^{-4} m^2 J^{-1}).[51] This approach afforded doses of 5–8 Gy per electron pulse, water equivalent.

The kinetic data presented were generated by averaging three individual measurements per sample, with each measurement consisting of eight individual pulses. The kinetic decay traces were fitted with a combination of two exponential decay functions, each incorporating contributions from recombination (eqn (4)) and from the DGA reaction with a radiolytic transient (eqn (2) and (3)):[52]

$$\mathrm{Abs}(t) = A_0((1-f)\exp(-(k_1 + [\mathrm{DGA}]k_{\mathrm{DGA}})t) + (f)\exp(-(k_2 + [\mathrm{DGA}]k_{\mathrm{DGA}})t)) + A_f, \quad (5)$$

where k_1 and k_2 are the decay rates of the *n*-dodecane radiolytic transients associated with geminate and non-geminate recombination pathways without DGAs present, f is the fraction of the transient that decays *via* non-geminate recombination, A_0 and A_f are the initial and final absorbances at the given wavelength, k_{DGA} is the pseudo-first-order decay rate of the reaction of the transient in *n*-dodecane with a DGA present, and [DGA] is the concentration of the DGA in *n*-dodecane. The parameter A_f accounts for a small constant component observed in the kinetic traces, indicating the presence of a residual species or background signal that prevents the absorbance from returning to baseline.

Fitting the kinetic traces in this manner accounts for both geminate and non-geminate recombination pathways and fixes the transient decays for *n*-dodecane, then considers the impact of the DGAs as an enhancement of these rates. Additionally, this method allows for the minimization of uncertainties by fitting all traces for a given DGA at a given temperature simultaneously. The quoted errors for the derived second-order rate coefficients and activation parameters are a combination of measurement precision (∼4%) and initial (∼1%) and dilution (<1%) sample concentration errors.

Cobalt-60 gamma dose accumulation irradiations

Dose accumulation studies were performed using a Foss Therapy Services (North Hollywood, CA, USA) Model 812 cobalt-60 self-contained gamma irradiator at the Idaho National Laboratory (INL) Center for Radiation Chemistry Research (CR2). Samples comprised of 5 mL of organic solution—50 mM DGA dissolved in neat *n*-dodecane—sealed in 20 mL screwcap borosilicate glass vials with an air headspace of 15 mL. Gamma irradiations were performed in triplicate to absorbed doses of up to 600 kGy. Dose rates (25–283 Gy min^{-1}) were determined for each occupied irradiator sample position by chemical dosimetry using Fricke solution (1 mM $FeSO_4{\cdot}7H_2O$ and 1 mM NaCl in 0.4 M H_2SO_4)[43,53] and an Agilent (Santa Clara, CA, USA) Cary 60 UV-vis spectrophotometer. The calculated absorbed doses were corrected for the radioactive decay of cobalt-60 ($\tau_{1/2}$ = 5.27 years, $E_{\gamma 1}$ = 1.17 MeV and $E_{\gamma 2}$ = 1.33 MeV) and the electron density difference of *n*-dodecane *vs.* Fricke solution: $(Z_{n\text{-dodecane}}/A_{n\text{-dodecane}})/(Z_{\mathrm{Fricke}}/A_{\mathrm{Fricke}})$ = 1.04, where Z and A are the atomic number and mass number, respectively.[43,53]

DGA degradation quantification

Following gamma irradiation, the remaining concentration of each DGA was quantified by gas chromatography (GC) using an Agilent 7890 Series II gas chromatograph equipped with a flame

ionization detector. The GC method employed here used a HP-5 capillary column (30 m × 0.32 mm ID × 0.25 μm df) with a constant injector temperature of 300 °C. Each sample run began with an initial oven temperature of 40 °C for a duration of 1 minute and then ramped to 325 °C at a rate of 30 °C min^{-1} and held for an additional 9 minutes. The detector temperature was held at 350 °C.

DGA samples were prepared for GC analysis by 1 : 50 dilution in *n*-hexane. Following dilution, each sample was vortex mixed for 30 seconds and then placed in an autosampler tray for analysis. Samples were injected in triplicate to account for variation in the sample, as well as for measurement of instrument errors. Standard solutions, comprising 0.2–2.0 mM DGA in *n*-dodecane/*n*-hexane, were used to create calibration curves (Tables S1–S3, and Fig. S23–S25, ESI†). Separate quality control (QC) samples, comprising 0.6–1.6 mM DGA in *n*-dodecane/*n*-hexane, were also integrated into the analysis sequence at the beginning and end of each batch of runs and after every 9–10 samples to account for any instrument drift or changes in signal peak position. All samples, standards, and QCs were prepared using Rainin (Oakland, CA, USA) positive-displacement pipettes ranging in volume from 1 μL to 1 mL. Errors in diluted sample concentrations were ∼7%.

Results and discussion

Spectra of dodecane radiolytic transients

Solutions of *n*-dodecane, either sparged with Ar or N_2O or containing 100 mM TEA, were prepared to identify the absorbance maxima of *n*-dodecane's primary radiolysis products, the e_{solv}^-, $RH^{\bullet+}$, and RH*, as shown in Fig. 2. Saturating *n*-dodecane with Ar removed dissolved oxygen, enabling the observation of all three primary radiolysis products (Fig. 2A). It is known that RH* has an absorbance maximum around 650 nm.[49] The spectrum for $RH^{\bullet+}$ (Fig. 2B) was isolated by saturating *n*-dodecane with N_2O, which is an excellent e_{solv}^- scavenger.[54] By scavenging the e_{solv}^-, charge recombination is inhibited (eqn (4)), thereby reducing the contributions of both the e_{solv}^- and RH* to the transient spectrum, resulting in an increased yield and absorption of $RH^{\bullet+}$, allowing for its isolation. By the same logic, TEA is an excellent $RH^{\bullet+}$ scavenger,[55] enabling the isolation of the e_{solv}^- spectrum in Ar-saturated *n*-dodecane (Fig. 2C). A minor contribution from the $RH^{\bullet+}$ spectrum is still observed 1–2 ns after the electron pulse, before being completely scavenged by 100 mM TEA.

The spectra presented in Fig. 2 are consistent with those previously reported by Tagawa *et al.* and Saeki *et al.*, who

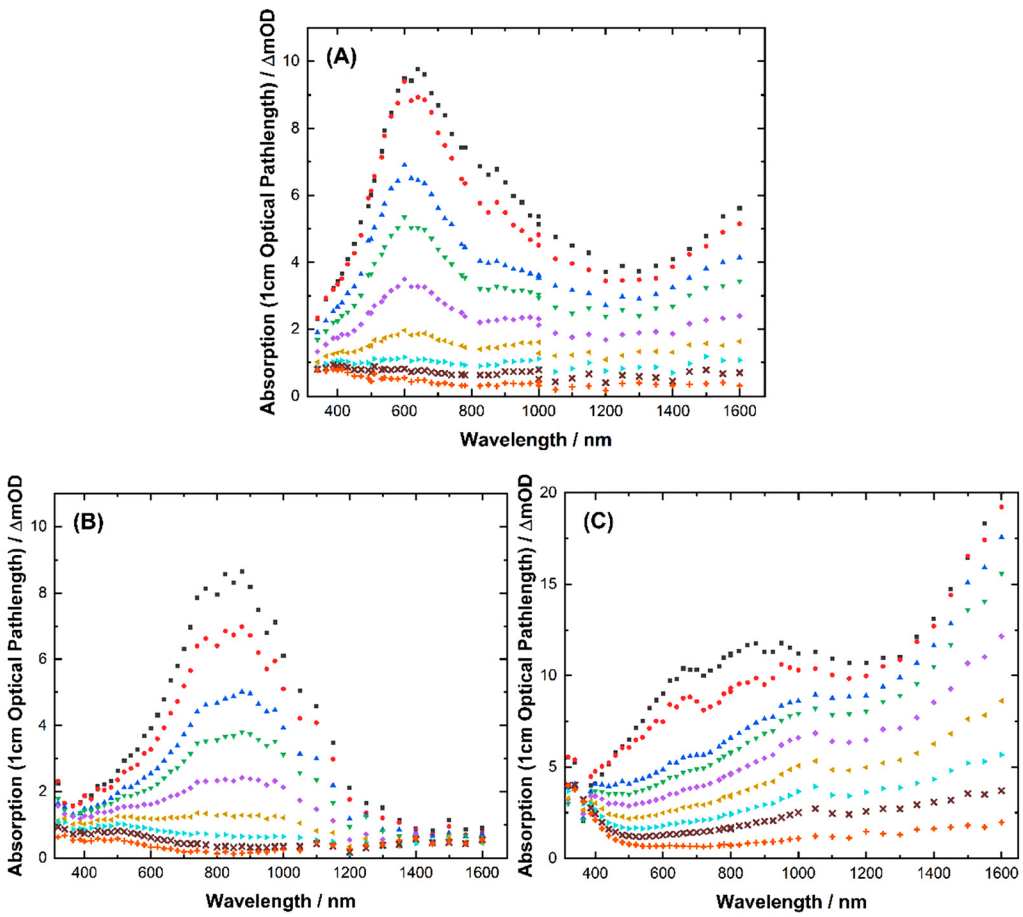

Fig. 2 Transient absorption spectra at 1 (■), 2 (●), 3 (▲), 4 (▼), 6 (◆), 10 (◀), 16 (▶), 25 (×), and 63 (+) ns after the electron pulse for *n*-dodecane: (A) saturated with Ar to show all three observable primary *n*-dodecane radiolysis products; (B) saturated with N_2O to isolate the $RH^{\bullet+}$ absorbance maximum; (C) Ar-saturated with the addition of 100 mM TEA to isolate the e_{solv}^- absorbance maximum.

assigned peaks to RH* and $RH^{\bullet+}$ at 650 and 850 nm, respectively.[49,56] They also demonstrated that the e_{solv}^- absorbs at the end of their spectra at 1600 nm. Our e_{solv}^- spectra are consistent with those reported in other lower carbon chain length organic solvents by Mostafavi and Isabelle[57] and Baxendale and Rasburn.[58] These studies also confirm that the e_{solv}^- in nonpolar, aliphatic organic solvents exhibits a large absorption band from ~1500–2375 nm, with a maximum absorbance around 1820 nm. As shown in Fig. 2, the detectors used here could measure up to 1600 nm, and this value was used to monitor the decay of the e_{solv}^-.

Based on the spectra shown in Fig. 2, the wavelengths chosen to directly analyze the decay kinetics of the e_{solv}^- and $RH^{\bullet+}$ in this study were 1600 and 850 nm, respectively. Within the investigated wavelength region, there was no observation of DGA radical anions or cations resulting from the e_{solv}^- and $RH^{\bullet+}$ reactions, respectively.

Reaction kinetics of DGA derivatives with the solvated electron

Decay traces for the e_{solv}^- in the presence of TODGA, T2EHDGA, and DMDODGA at varying concentrations are shown in Fig. 3. These traces indicate that the e_{solv}^- decay rate increases with increasing concentration of DGA. Additionally, the e_{solv}^- decay rate also increases with temperature, as demonstrated in Fig. 4A for 1 mM DMDODGA. Both trends are consistent with previous temperature-controlled measurements reported for TODGA with the $RH^{\bullet+}$.[31,44] Additional e_{solv}^- decay trace plots for each concentration of DGA and temperature are provided in the ESI,† Fig. S5–S15. To the authors' knowledge, these are the first measurements for the reaction of the e_{solv}^- with a reprocessing ligand in *n*-dodecane. Second-order rate coefficients (k_{DGA}) for the e_{solv}^- reaction with TODGA, T2EHDGA, and DMDODGA were derived from fits to data measured at 10.0–44.1 °C starting at 2 ns after the electron pulse, according to eqn (5). These k_{DGA} values are summarized in Table 1.

These new data indicate that the e_{solv}^- reacts fastest with DMDODGA; however, the overall reaction rates are similar between the DGAs. The faster reaction with DMDODGA may be attributed to its more accessible polar backbone, as DMDODGA has one shorter unbranched chain compared to TODGA and T2EHDGA (Fig. 1). These observations suggest that increasing the chain length from a methyl to an octyl group may provide slightly more radiation protection by sterically limiting direct access to the central backbone. This observation further supports the argument made by Horne *et al.*[31] that the mechanisms responsible for the degradation of a DGA are similar, and that they most likely involve the more polar backbone of the DGA extractant. Overall, the same mechanisms could be responsible for the degradation of DGA extractants, with only slight variation in rate.

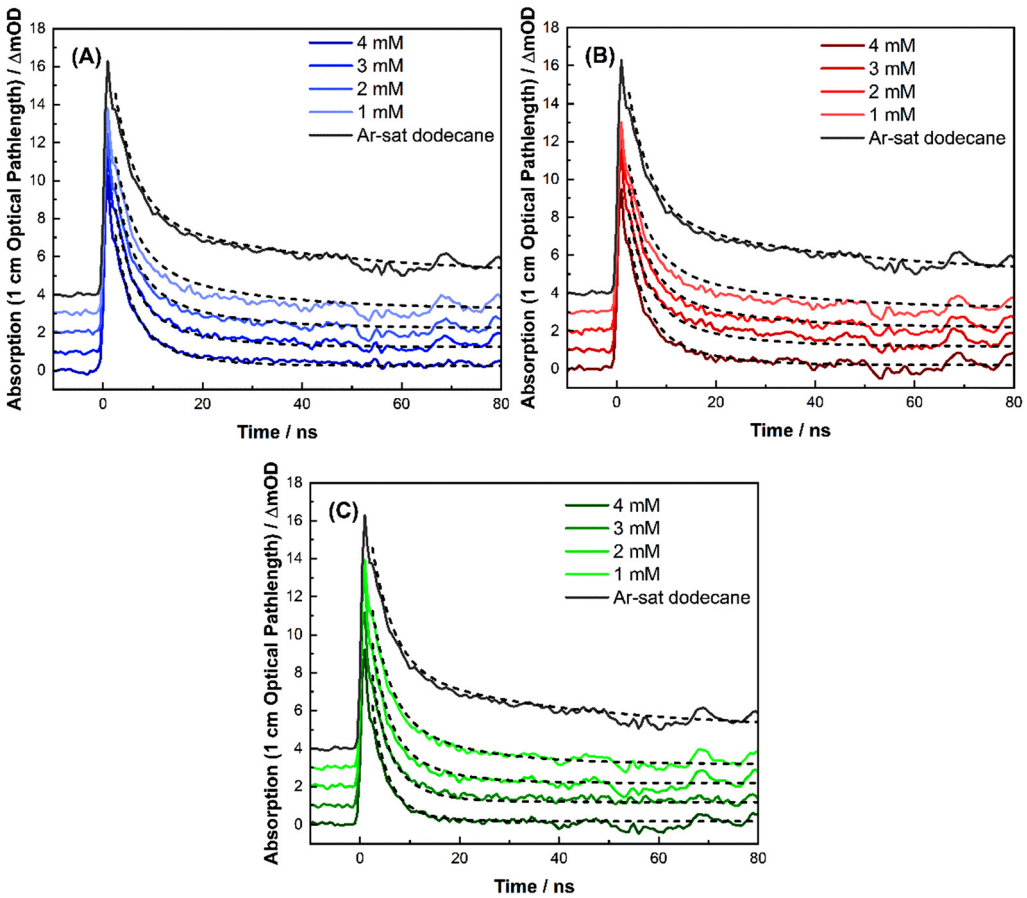

Fig. 3 Kinetic traces at 1600 nm for the interaction between the e_{solv}^- and 1, 2, 3, and 4 mM (A) TODGA (▪), (B) T2EHDGA (▪), and (C) DMDODGA (▪) in *n*-dodecane at 20.0 °C. Traces were offset by 1 mOD to aid in visibility of the reaction kinetics. Fits with eqn (5) are shown by the dashed lines (- -).

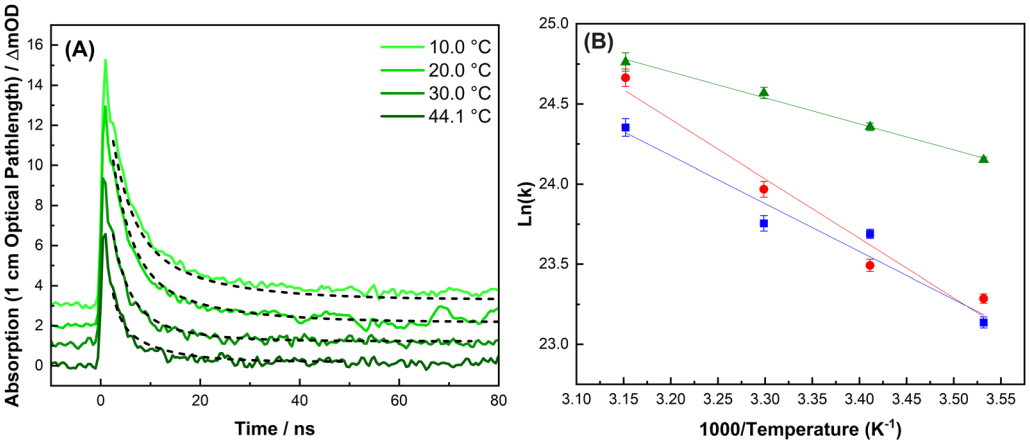

Fig. 4 (A) Dose normalized kinetic traces at 1600 nm for the decay of the e_{solv}^- from 10.0 to 44.1 °C for 1 mM DMDODGA. Traces are offset by 1 mOD to aid in visibility. Traces were fitted with a combination of two exponential functions, shown by the dashed black lines. (B) Arrhenius plots for the reaction of the e_{solv}^- with TODGA (■), T2EHDGA (●), and DMDODGA (▲): $E_a(e_{solv}^- + \text{TODGA}) = 24.85 \pm 4.20$ kJ mol^{-1}, $E_a(e_{solv}^- + \text{T2EHDGA}) = 30.85 \pm 4.24$ kJ mol^{-1}, and $E_a(e_{solv}^- + \text{DMDODGA}) = 13.53 \pm 0.74$ kJ mol^{-1}. Individual data points are from the second-order rate coefficients found at 10.0, 20.0, 30.0, and 44.1 °C.

Table 1 Calculated second-order rate coefficients (k_{DGA}) and Arrhenius (E_a and A) parameters for the reaction between the studied DGAs and the e_{solv}^-

	Second-order rate coefficient for e_{solv}^- + DGA ($k_{DGA}/10^{10}$ M^{-1} s^{-1})					
DGA	10.0 °C	20.0 °C	30.0 °C	44.1 °C	E_a (kJ mol^{-1})	Ln(A)
TODGA	1.12 ± 0.04	1.94 ± 0.06	2.07 ± 0.10	3.77 ± 0.21	24.85 ± 4.20	33.74 ± 1.69
T2EHDGA	1.30 ± 0.04	1.59 ± 0.06	2.57 ± 0.13	5.14 ± 0.28	30.85 ± 4.24	36.28 ± 1.71
DMDODGA	3.08 ± 0.05	3.78 ± 0.09	4.68 ± 0.17	5.67 ± 0.32	13.53 ± 0.74	29.91 ± 0.30

Reaction kinetics of DGA derivatives with the dodecane radical cation

Similar to the behavior of the e_{solv}^-, the lifetime of the $RH^{\bullet+}$ decreases with increasing DGA concentration and temperature. The $RH^{\bullet+}$ decay traces for each DGA concentration and temperature are provided in the ESI,† Fig. S16–S23. The fitted rate coefficients for each DGA are summarized in Table 2, demonstrating the same trend in relative chemical reactivity as observed for the e_{solv}^-, with DMDODGA reacting faster than T2EHDGA. These observations again suggest that increasing the chain length from a methyl to an octyl group offers slightly more radiation robustness.

The second-order rate coefficient values for TODGA with the $RH^{\bullet+}$ from Horne *et al.*[31] and Mezyk *et al.*[44] in Table 2 are not within the range of each other's uncertainties. Additionally, a publication by Zarzana *et al.*[12] reports a second-order rate coefficient value of $(0.97 \pm 0.11) \times 10^{10}$ M^{-1} s^{-1} at room temperature (20.0–23.0 °C), which is similar to Mezyk *et al.*[44] The value reported by Deokar *et al.*[19] was found to be $(2.38 \pm 0.15) \times 10^{10}$ M^{-1} s^{-1}, which is higher than all of the values reported. In fact, the TODGA measurements at ambient temperature span a range of values from $(0.9–2.4) \times 10^{10}$ M^{-1} s^{-1}. This variation in reaction rate may be due to differences in the DGA batch purities between the studies, or inconsistencies in fitting such short-timescale reactions accurately, which the use of eqn (5) in this study is designed to overcome.

Temperature effects on DGA reaction kinetics

Arrhenius plots of the e_{solv}^- and $RH^{\bullet+}$ reactions with the DGAs are shown in Fig. 4B and Fig. S1 (ESI†), respectively, allowing for calculation of the corresponding activation energies (E_a) and pre-exponential factors (A), which are summarized in Tables 1 and 2. The E_a value indicates the energy barrier that must be overcome for a given DGA and radiolysis product to react, offering insights into how molecular architecture may be tailored to influence this barrier. When comparing E_a values for the $RH^{\bullet+}$ in Table 1, DMDODGA has the lowest and T2EHDGA has the highest, while values reported for TODGA by Horne *et al.*[31] (17.43 ± 1.64 kJ mol^{-1}) and Mezyk *et al.*[44] (20.40 ± 0.70 kJ mol^{-1}) fall in between. The E_a values for the reaction of the e_{solv}^- with the studied DGAs follow the same order as those for the $RH^{\bullet+}$ reactions: DMDODGA < TODGA < T2EHDGA. The ordering of these activation energies corresponds directly with the order of steric hinderance, further indicating that the observed differences in chemical reactivity are correlated with DGA structure.

Impact of DGA molecular architecture on dose accumulation effects

Dose accumulation irradiations were performed to evaluate whether the observed effects of DGA molecular architecture on the initial chemical kinetics translate to accelerating or decelerating ligand degradation rates over longer timescales relevant to UNF reprocessing, thereby addressing discrepancies in previous literature.[12,45] Concentrations of each DGA from this study, along with those reported by Horne *et al.*[32] and Zarzana *et al.*,[12] are shown in Fig. 5 as a function of absorbed gamma dose, and were calculated using the data in Tables S4–S6 (ESI†). The data from Zarzana *et al.*[12] were recalculated to account for the difference in electron density between Fricke solution and

Table 2 Calculated second-order rate coefficients (k_{DGA}) and Arrhenius (E_a and A) parameters for the reaction between the studied DGAs and the $RH^{\bullet+}$ alongside previously reported values for TODGA[31,44]

	Second-order rate coefficient for $RH^{\bullet+}$ + DGA ($k_{DGA}/10^{10}$ M^{-1} s^{-1})					
DGA	8.9 °C	21.0 °C	31.0 °C	40.7 °C	E_a (kJ mol^{-1})	ln(A)
TODGA[31]	1.20 ± 0.34	1.57 ± 0.28	1.91 ± 0.51	2.61 ± 0.49	17.43 ± 1.64	30.79 ± 0.02
	10.0 °C	**20.0 °C**	**30.0 °C**	**40.0 °C**	$\boldsymbol{E_a}$ (kJ mol^{-1})	**ln(A)**
TODGA[44]	0.62 ± 0.09	0.86 ± 0.10	1.12 ± 0.07	1.41 ± 0.31	20.40 ± 0.69	31.23 ± 0.27
	10.0 °C	**20.0 °C**	**30.0 °C**	**44.1 °C**	$\boldsymbol{E_a}$ (kJ mol^{-1})	**ln(A)**
T2EHDGA	0.59 ± 0.04	1.00 ± 0.05	1.29 ± 0.10	2.24 ± 0.19	28.25 ± 2.21	34.54 ± 0.89
DMDODGA	1.20 ± 0.03	1.61 ± 0.04	2.00 ± 0.10	2.56 ± 0.20	16.50 ± 1.03	30.24 ± 0.42

n-dodecane (1.04).[43] All the DGAs shown degrade exponentially with absorbed gamma dose, with subtle indications that T2EHDGA is more radiolytically robust than both DMDODGA and TODGA.

The dose constants derived from these data are shown in Table 3. These values were calculated from the slope of linear fits plotted in Fig. S2 (ESI†). The loss of T2EHDGA with absorbed gamma dose was indeed less than both DMDODGA and TODGA, indicating that shortening of the DGA R-group chain has a negligible effect on the overall degradation rate of the molecule at long-timescales (>5 nanoseconds), while branching chains confer marginal additional stability. These observations are in agreement with the recalculated value reported by Zarzana *et al.*[12] (3.67 ± 0.23 × 10^{-3} kGy^{-1}) to within the experimental uncertainty.

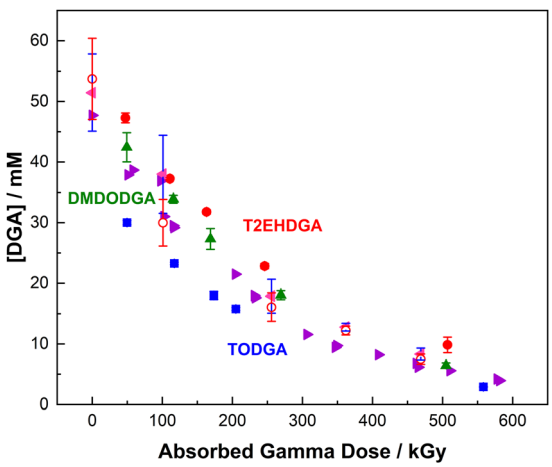

Fig. 5 DGA concentrations as a function of absorbed gamma dose in *n*-dodecane: TODGA (■), T2EHDGA (●), and DMDODGA (▲) from this work. Previously reported values for: TODGA (▶),[32] TODGA (◀),[12] and corrected for the electron density difference between Fricke and *n*-dodecane (1.04).

The similarity in DGA dose constants suggests that despite differences in chemical kinetics, the fate of the radical DGA products formed by eqn (2) and (3) are predominantly dictated by the fragmentation chemistry of the backbone structure common to all three studied DGAs.

The TODGA dose constant determined here (4.65 ± 0.09 × 10^{-3} kGy^{-1}) is higher than those reported by Zarzana *et al.*[12] (4.07 ± 0.25 × 10^{-3} kGy^{-1}) and Horne *et al.*[32] (4.36 ± 0.08 × 10^{-3} kGy^{-1}). This could suggest that different batches of DGAs result in varying dose constant values for the same extractant, as the DGA batches reported here and in literature range from >97% to >99% purity. Minute changes in composition and/or purity of a DGA batch may have a role in the degradation or radioprotection of a DGA in *n*-dodecane.

Conclusions

Time-resolved electron pulse and steady-state gamma irradiations of TODGA, T2EHDGA, and DMDODGA in *n*-dodecane examined whether changes in DGA molecular architecture significantly influence their extent of radiolytic degradation. Time-resolved experiments determined rate coefficients for the reactions of the e_{solv}^- and $RH^{\bullet+}$ with each DGA, demonstrating that reaction rates increased with increasing temperature, DGA concentration, and reduced steric hindrance around the DGA backbone.[31] Arrhenius parameters, specifically the E_a for each reaction (DMDODGA < TODGA < T2EHDGA), further support the theory that access to the DGA backbone is an essential mechanistic step in initiating radical damage at short timescales.

Steady-state irradiations indicate that the branching chains in T2EHDGA may have provided slight radioprotection relative to TODGA and DMDODGA. However, given the similarities in rate coefficients and dose constants between all three investigated

Table 3 Summary of derived dose constants for the cobalt-60 gamma irradiation of 50 mM DGA in *n*-dodecane. The referenced values were recalculated using the raw data acquired from their respective publications to account for the electron density difference between *n*-dodecane and Fricke solution

DGA	Dose constant (10^{-3} kGy^{-1})	Comments
TODGA[12]	4.07 ± 0.25	Unknown purity, recalculated from raw data
TODGA[32]	4.36 ± 0.08	99% purity, recalculated from raw data
TODGA (this work)	4.65 ± 0.09	97% purity
T2EHDGA[12]	3.67 ± 0.23	Unknown purity, recalculated from raw data
T2EHDGA (this work)	3.41 ± 0.07	≥97% purity
DMDODGA (this work)	4.19 ± 0.09	≥97% purity

DGAs, their degradation is likely occurring *via* the same mechanisms, and any radioprotection conferred by modifying their chain structures is minimal. Differences in dose constants between various reported studies of TODGA also indicate that the purity of a DGA may also contribute to the rate at which it degrades.

Overall, our findings suggest that more extensive modifications to the DGA molecular architecture are necessary to achieve significant differences in radiation robustness under envisioned UNF reprocessing conditions. Follow-up experiments will assess the radiolytic interplay of metal ion complexation, the presence of other ubiquitous UNF reprocessing solutes, like HNO_3 and O_2, and changes in DGA molecular architecture.

Data availability

The data supporting this article have been included as part of the ESI.†

Note added after first publication

This article replaces the original version published on 18th July 2025, which contained errors in the presented dose rate values.

Conflicts of interest

The authors declare no conflicts of interest.

Acknowledgements

Bronstetter and Gaiser were supported by MSU startup funds. Conrad, Mezyk, and Wilbanks were supported through the INL Laboratory Directed Research & Development (LDRD) Program under DOE Idaho Operations Office Contract DE-AC07-05ID14517. Horne was supported by the U.S. DOE, Office of Science, Office of Basic Energy Sciences, Solar Photochemistry Program under award DE-SC0024191. Cook, Layne, and electron pulse irradiation experiments at the LEAF of the BNL Accelerator Center for Energy Research were supported by the U.S. DOE, BES, Division of Chemical Sciences, Geosciences, and Biosciences under contract DE-SC0012704.

References

1 E. R. Irish and W. H. Reas, *The PUREX Process - A Solvent Extraction Reprocessing Method for Irradiated Uranium*, Richland, Washington, 1957.
2 S. Bourg, C. Hill, C. Caravaca, C. Rhodes, C. Ekberg, R. Taylor, A. Geist, G. Modolo, L. Cassayre, R. Malmbeck, M. Harrison, G. de Angelis, A. Espartero, S. Bouvet and N. Ouvrier, ACSEPT—Partitioning Technologies and Actinide Science: Towards Pilot Facilities in Europe, *Nucl. Eng. Des.*, 2011, **241**, 3427–3435.
3 C. Madic, F. Testard, M. J. Hudson, J. O. Liljenzin, B. Christiansen, M. Ferrando, A. Facchini, A. Geist, G. Modolo, A. Gonzalez-Espartero and J. de Mendoza, *Partnew – New solvent extraction processes for minor actinides – final report*, 2004, preprint, https://inis.iaea.org/search/search.aspx?orig_q=RN:36033048.
4 K. Nash, C. Madic, J. Mathur and J. Lacquement, in *The Chemistry of the Actinides and Transactinide Elements*, ed. L. Morss, N. Edelstein, J. Fuger and J. Katz, Springer, The Netherlands, 3rd edn, 2006, vol. 4, p. 2622.
5 S. A. Ansari, P. Pathak, P. K. Mohapatra and V. K. Manchanda, Aqueous Partitioning of Minor Actinides by Different Processes, *Sep. Purif. Rev.*, 2011, **40**, 43–76.
6 V. K. Manchanda and P. N. Pathak, Amides and Diamides as Promising Extractants in the Back End of the Nuclear Fuel Cycle: An Overview, *Sep. Purif. Technol.*, 2004, **35**, 85–103.
7 C. Madic and N. Ouvrier, EUROPART: EUROpean Research Program for the PARTitioning of Minor Actinides from High Active Wastes Arising from the Reprocessing of Spent Nuclear Fuels, *Radiochim. Acta*, 2008, **96**, 183–185.
8 C. Musikas, Solvent Extraction for the Chemical Separations of the 5f Elements, *Inorg. Chim. Acta*, 1987, **140**, 197–206.
9 D. Serrano-Purroy, P. Baron, B. Christiansen, J.-P. Glatz, C. Madic, R. Malmbeck and G. Modolo, First Demonstration of a Centrifugal Solvent Extraction Process for Minor Actinides from a Concentrated Spent Fuel Solution, *Sep. Purif. Technol.*, 2005, **45**, 157–162.
10 S. A. Ansari, P. Pathak, P. K. Mohapatra and V. K. Manchanda, Chemistry of Diglycolamides: Promising Extractants for Actinide Partitioning, *Chem. Rev.*, 2012, **112**, 1751–1772.
11 G. P. Horne, C. A. Zarzana, T. S. Grimes, C. Rae, J. Ceder, S. P. Mezyk, B. J. Mincher, M.-C. Charbonnel, P. Guilbaud, G. Saint-Louis and L. Berthon, Effect of Chemical Environment on the Radiation Chemistry of N,N-di-(2-ethylhexyl)butyramide (DEHBA) and Plutonium Retention, *Dalton Trans.*, 2019, **48**, 14450–14460.
12 C. A. Zarzana, G. S. Groenewold, B. J. Mincher, S. P. Mezyk, A. Wilden, H. Schmidt, G. Modolo, J. F. Wishart and A. R. Cook, A Comparison of the γ-Radiolysis of TODGA and T(EH)DGA Using UHPLC-ESI-MS Analysis, *Solvent Extr. Ion Exch.*, 2015, **33**, 431–447.
13 S. P. Mezyk, G. P. Horne, B. J. Mincher, P. R. Zalupski, A. R. Cook and J. F. Wishart, The Chemistry of Separations Ligand Degradation by Organic Radical Cations, *Procedia Chem.*, 2016, **21**, 61–65.
14 T. Toigawa, D. R. Peterman, D. S. Meeker, T. S. Grimes, P. R. Zalupski, S. P. Mezyk, A. R. Cook, S. Yamashita, Y. Kumagai, T. Matsumura and G. P. Horne, Radiation-Induced Effects on the Extraction Properties of Hexa- *n* -octylnitrilotriacetamide (HONTA) Complexes of Americium and Europium, *Phys. Chem. Chem. Phys.*, 2021, **23**, 1343–1351.
15 C. Celis Barros, C. D. Pilgrim, A. R. Cook, S. P. Mezyk, T. S. Grimes and G. P. Horne, Influence of Uranyl Cpmplexation on the Reaction Kinetics of the Dodecane Radical Cation with Used Nuclear Fuel Extraction Ligands (TBP, DEHBA, and DEHiBA), *Phys. Chem. Chem. Phys.*, 2021, **23**, 24589–24597.
16 S. P. Mezyk, B. J. Mincher, S. B. Dhiman, B. Layne and J. F. Wishart, The Role of Organic Solvent Radical Cations in Separations Ligand Degradation, *J. Radioanal. Nucl. Chem.*, 2016, **307**, 2445–2449.

17 J. Drader, G. Saint-Louis, J. M. Muller, M.-C. Charbonnel, P. Guilbaud, L. Berthon, K. M. Roscioli-Johnson, C. A. Zarzana, C. Rae, G. S. Groenewold, B. J. Mincher, S. P. Mezyk, K. McCann, S. G. Boyes and J. Braley, Radiation Chemistry of the Branched-chain Monoamide Di-2-ethylhexyl-isobutyramide, *Solvent Extr. Ion Exch.*, 2017, **35**, 480–495.

18 G. P. Horne, A. Wilden, S. P. Mezyk, L. Twight, M. Hupert, A. Stärk, W. Verboom, B. J. Mincher and G. Modolo, Gamma Radiolysis of Hydrophilic Diglycolamide Ligands in Concentrated Aqueous Nitrate Solution, *Dalton Trans.*, 2019, **48**, 17005–17013.

19 R. G. Deokar and A. R. Cook, Early-stage Oxidation and Subsequent Damage of the Used Nuclear Fuel Extractant TODGA; Electron Pulse Radiolysis and Theoretical Insights, *Phys. Chem. Chem. Phys.*, 2024, **26**, 29060–29069.

20 A. Kimberlin, G. Saint-Louis, D. Guillaumont, B. Camès, P. Guilbaud and L. Berthon, Effect of Metal Complexation on Diglycolamide Radiolysis: A Comparison Between Ex Situ Gamma and In Situ Alpha Irradiation, *Phys. Chem. Chem. Phys.*, 2022, **24**, 9213–9228.

21 A. Kimberlin, D. Guillaumont, S. Arpigny, B. Camès, P. Guilbaud, G. Saint-Louis, H. Galán and L. Berthon, An Experimental and Computational Look at the Radiolytic Degradation of TODGA and the Effect on Metal Complexation, *New J. Chem.*, 2021, **45**, 12479–12493.

22 I. Sánchez-García, R. J. M. Egberink, W. Verboom and H. Galán, Radiolytic Stability and Effects on Metal Extraction of *N*,*N*,*N*′,*N*′-trioctyldiglycolamide, an Important TODGA Degradation Product, *New J. Chem.*, 2024, **48**, 2087–2096.

23 Y. Sasaki, Y. Sugo, S. Suzuki and S. Tachimori, The Novel Extractants, Diglycolamides, for the Extraction of Lanthanides and Actinides in HNO_3–*n*-Dodecane System, *Solvent Extr. Ion Exch.*, 2001, **19**, 91–103.

24 I. Sánchez-García and H. Galán, Effect of Europium Complexation on N,N,N′,N′-Tetraoctyldiglycolamide Degradation Against Gamma Radiation, *Arabian J. Sci. Eng.*, 2025, **50**, 3145–3153.

25 H. Zhang, Y.-Y. Ao, Y. Wang, S.-J. Zhao, J.-Y. Sun, M.-L. Zhai, J.-Q. Li, J. Peng and H.-B. Li, Effect of Radiolysis of TODGA on the Extraction of TODGA/n-dodecane Toward Eu(III): An Experimental and DFT Study, *Nucl. Sci. Tech.*, 2023, **34**, 48.

26 I. Sánchez-García, H. Galán, J. M. Perlado and J. Cobos, Development of Experimental Irradiation Strategies to Evaluate the Robustness of TODGA and Water-soluble BTP Extraction Systems for Advanced Nuclear Fuel Recycling, *Radiat. Phys. Chem.*, 2020, **177**, 109094.

27 I. Sánchez-García, H. Galán, J. M. Perlado and J. Cobos, Stability Studies of GANEX System Under Different Irradiation Conditions, *EPJ Nucl. Sci. Technol.*, 2019, **5**, 19.

28 H. Galán, A. Núñez, A. G. Espartero, R. Sedano, A. Durana and J. de Mendoza, Radiolytic Stability of TODGA: Characterization of Degraded Samples under Different Experimental Conditions, *Procedia Chem.*, 2012, **7**, 195–201.

29 B. Verlinden, K. Van Hecke, A. Wilden, M. Hupert, B. Santiago-Schübel, R. J. M. Egberink, W. Verboom, P. M. Kowalski, G. Modolo, M. Verwerft, K. Binnemans and T. Cardinaels, Gamma Radiolytic Stability of the Novel Modified Diglycolamide 2,2′-oxybis(*N*,*N*-didecylpropanamide) (mTDDGA) for Grouped Actinide Extraction, *RSC Adv.*, 2022, **12**, 12416–12426.

30 C. A. Zarzana, J. McAlpine, A. Wilden, M. Hupert, A. Stärk, M. Iqbal, W. Verboom, A. N. Vandevender, B. J. Mincher, G. S. Groenewold and G. Modolo, Gamma Radiolysis of Phenyl-Substituted TODGAs: Part II, *Solvent Extr. Ion Exch.*, 2023, **41**, 582–605.

31 G. P. Horne, C. Celis-Barros, J. K. Conrad, T. S. Grimes, J. R. McLachlan, B. M. Rotermund, A. R. Cook and S. P. Mezyk, Impact of Lanthanide Ion Complexation and Temperature on the Chemical Reactivity of *N*,*N*,*N*′,*N*′-tetraoctyl diglycolamide (TODGA) with the Dodecane Radical Cation, *Phys. Chem. Chem. Phys.*, 2023, **25**, 16404–16413.

32 G. P. Horne, C. A. Zarzana, C. Rae, A. R. Cook, S. P. Mezyk, P. R. Zalupski, A. Wilden and B. J. Mincher, Does Addition of 1-octanol as a Phase Modifier Provide Radical Scavenging Radioprotection for *N*,*N*,*N*′,*N*′-tetraoctyldiglycolamide (TODGA)?, *Phys. Chem. Chem. Phys.*, 2020, **22**, 24978–24985.

33 A. Wilden, B. J. Mincher, S. P. Mezyk, L. Twight, K. M. Rosciolo-Johnson, C. A. Zarzana, M. E. Case, M. Hupert, A. Stärk and G. Modolo, Radiolytic and Hydrolytic Degradation of the Hydrophilic Diglycolamides, *Solvent Extr. Ion Exch.*, 2018, **36**, 347–359.

34 P. R. Zalupski and D. R. Peterman, *Evaluation of ALSEPO*, Idaho Falls, ID (United States), 2017.

35 D. Peterman, A. Geist, B. Mincher, G. Modolo, M. H. Galán, L. Olson and R. McDowell, Performance of an i-SANEX System Based on a Water-Soluble BTP under Continuous Irradiation in a γ-Radiolysis Test Loop, *Ind. Eng. Chem. Res.*, 2016, **55**, 10427–10435.

36 K. M. Roscioli-Johnson, C. A. Zarzana, G. S. Groenewold, B. J. Mincher, A. Wilden, H. Schmidt, G. Modolo and B. Santiago-Schübel, A Study of the γ-Radiolysis of N,N-Didodecyl-N′,N′-Dioctyldiglycolamide Using UHPLC-ESI-MS Analysis, *Solvent Extr. Ion Exch.*, 2016, **34**, 439–453.

37 A. Wilden, G. Modolo, P. Kaufholz, F. Sadowski, S. Lange, M. Sypula, D. Magnusson, U. Müllich, A. Geist and D. Bosbach, Laboratory-Scale Counter-Current Centrifugal Contactor Demonstration of an Innovative-SANEX Process Using a Water Soluble BTP, *Solvent Extr. Ion Exch.*, 2015, **33**, 91–108.

38 J. Ravi, K. A. Venkatesan, M. P. Antony, T. G. Srinivasan and P. R. Vasudeva Rao, Solvent Extraction Behavior of Trivalent Metal Ions in Diglycolamides Having Same Carbon to Oxygen Ratio, *Sep. Sci. Technol.*, 2016, **51**, 32–40.

39 H. Galán, C. A. Zarzana, A. Wilden, A. Núñez, H. Schmidt, R. J. M. Egberink, A. Leoncini, J. Cobos, W. Verboom, G. Modolo, G. S. Groenewold and B. J. Mincher, Gamma-Radiolytic Stability of New Methylated TODGA Derivatives for Minor Actinide Recycling, *Dalton Trans.*, 2015, **44**, 18049–18056.

40 Y. Sasaki, Y. Sugo, Y. Kitatsuji, A. Kirishima, T. Kimura and G. R. Choppin, Complexation and Back Extraction of Various Metals by Water-soluble Diglycolamide, *Anal. Sci.*, 2007, **23**, 727–731.

41 G. Modolo, H. Asp, C. Schreinemachers and H. Vijgen, Development of a TODGA based Process for Partitioning of Actinides from a PUREX Raffinate Part I: Batch Extraction

Optimization Studies and Stability Tests, *Solvent Extr. Ion Exch.*, 2007, **25**, 703–721.

42 Y. Sugo, Y. Sasaki and S. Tachimori, Studies on Hydrolysis and Radiolysis of *N*,*N*,*N*′,*N*′-tetraoctyl-3-oxapentane-1,5-diamide, *Radiochim. Acta*, 2002, **90**, 161.

43 J. Spinks and R. Woods, *An Introduction to Radiation Chemistry*, Wiley and Sons, New York, 3rd edn, 1991.

44 M. H. Rogalski, A. N. Dang and S. P. Mezyk, Evaluation of the Arrhenius Behavior of *n* -dodecane Radical Cation ($RH^{\bullet+}$) Reactivity with Lanthanide Ion-Complexed *N*,*N*,*N*′,*N*′-tetraoctyl diglycolamide (TODGA), *Phys. Chem. Chem. Phys.*, 2025, **27**, 1960–1967.

45 P. Deepika, K. N. Sabharwal, T. G. Srinivasan and P. R. Vasudeva Rao, Studies on the use of *N*,*N*,*N*′,*N*′ -Tetra(2-Ethylhexyl) Diglycolamide (TEHDGA) for Actinide Partitioning II: Investigation on Radiolytic Stability, *Solvent Extr. Ion Exch.*, 2011, **29**, 230–246.

46 R. B. Gujar, S. A. Ansari, A. Bhattacharyya, P. K. Mohapatra, A. S. Kanekar, P. N. Pathak and V. K. Manchanda, Studies on the Radiolytic Stability of N,N,N′,N′-tetra-2-ethylhexyl Diglycolamide in n-Dodecane Solution Containing Different Phase Modifiers, *J. Radioanal. Nucl. Chem.*, 2011, **288**, 621–627.

47 J. N. Sharma, R. Ruhela, K. K. Singh, M. Kumar, C. Janardhanan, P. V. Achutan, S. Manohar, P. K. Wattal and A. K. Suri, Studies on Hydrolysis and Radiolysis of Tetra(2-ethylhexyl)diglycolamide (TEHDGA)/Isodecyl Alcohol/*n* -Dodecane Solvent System, *Radiochim. Acta*, 2010, **98**, 485–491.

48 J. F. Wishart, A. R. Cook and J. R. Miller, The LEAF Picosecond Pulse Radiolysis Facility at Brookhaven National Laboratory, *Rev. Sci. Instrum.*, 2004, **75**, 4359–4366.

49 S. Tagawa, N. Hayashi, Y. Yoshida, M. Washio and Y. Tabata, Pulse Radiolysis Studies on Liquid Alkanes and Related Polymers, *Radiat. Phys. Chem.*, 1989, **34**, 503–511.

50 R. Mehnert, O. Brede and W. Naumann, Spectral Properties and Kinetics of Cationic Transients Generated in Electron-Pulse Irradiated Liquid Alkanes, *J. Radioanal. Nucl. Chem.*, 1986, **101**, 307–318.

51 A. R. Cook, M. J. Bird, S. Asaoka and J. R. Miller, Rapid ''Step Capture'' of Holes in Chloroform during Pulse Radiolysis, *J. Phys. Chem. A*, 2013, **117**, 7712–7720.

52 J. K. Conrad, H. Hlushko and A. R. Cook, Kinetics for the Reaction between the Solvated Electron and Dissolved Oxygen in n-dodecane from 2.5 to 40 °C, *Radiat. Phys. Chem.*, 2025, **230**, 112587.

53 H. Fricke and E. J. Hart, The Oxidation of Fe++ to Fe+++ by the Irradiation with X-Rays of Solutions of Ferrous Sulfate in Sulfuric Acid, *J. Chem. Phys.*, 1935, **3**, 60–61.

54 S. Sato, R. Yugeta, K. Shinsaka and T. Terao, Nitrous Oxide as an Electron Scavenger in the Radiolysis of Hydrocarbons, *Bull. Chem. Soc. Jpn.*, 1966, **39**, 156–160.

55 M. Washio, S. Tagawa and Y. Tabata, Direct Observation of the Kinetic Behavior of a Charge-Transfer Reaction on the Cation-Scavenging Reaction for Cation Radicals of N-vinylcarbazole and N-ethylcarbazole by using a Pulse Radiolysis Technique, *J. Phys. Chem.*, 1980, **84**, 2876–2879.

56 A. Saeki, N. Yamamoto, Y. Yoshida and T. Kozawa, Geminate Charge Recombination in Liquid Alkane with Concentrated CCl_4: Effects of CCl_4 Radical Anion and Narrowing of Initial Distribution of Cl^-, *J. Phys. Chem. A*, 2011, **115**, 10166–10173.

57 M. Mostafavi and L. Isabelle, in *Radiation Chemistry: From Basics to Applications in Material and Life Sciences*, ed. M. Spotheim-Maurizot, M. Mostafavi, T. Douki and J. Belloni, EPD Sciences, France, 1st edn, 2008, pp. 35–52.

58 J. H. Baxendale and E. J. Rasburn, Pulse Radiolysis Study of the Kinetics of Electron Reactions in Liquid n-hexane at Room Temperature, *J. Chem. Soc., Faraday Trans. 1*, 1974, **70**, 705–717.